Predicting global average thermospheric temperature changes resulting from auroral heating

D. R. Weimer,[1] B. R. Bowman,[2] E. K. Sutton,[3] and W. K. Tobiska[4]

Received 17 May 2010; revised 7 September 2010; accepted 21 October 2010; published 25 January 2011.

[1] The total Poynting flux flowing into both polar hemispheres as a function of time, computed with an empirical model, is compared with measurements of neutral densities in the thermosphere at two altitudes obtained from accelerometers on the CHAMP and GRACE satellites. The Jacchia-Bowman 2008 empirical thermospheric density model (JB2008) is used to facilitate the comparison. This model calculates a background level for the "global nighttime minimum exospheric temperature," T_c, from solar indices. Corrections to this background level due to auroral heating, ΔT_c, are presently computed from the *Dst* index. A proxy measurement of this temperature difference, ΔT_c, is obtained by matching the CHAMP and GRACE density measurements with the JB2008 model. Through the use of a differential equation, the ΔT_c correction can be predicted from IMF values. The resulting calculations correlate very well with the orbit-averaged measurements of ΔT_c, and correlate better than the values derived from *Dst*. Results indicate that the thermosphere cools faster following time periods with greater ionospheric heating. The enhanced cooling is likely due to nitric oxide (NO) that is produced at a higher rate in proportion to the ionospheric heating, and this effect is simulated in the differential equations. As the ΔT_c temperature correction from this model can be used as a direct substitute for the *Dst*-derived correction that is now used in JB200, it could be possible to predict ΔT_c with greater accuracy and lead time.

Citation: Weimer, D. R., B. R. Bowman, E. K. Sutton, and W. K. Tobiska (2011), Predicting global average thermospheric temperature changes resulting from auroral heating, *J. Geophys. Res.*, *116*, A01312, doi:10.1029/2010JA015685.

1. Introduction

[2] The interaction of the solar wind and the embedded interplanetary magnetic field (IMF) with the Earth's magnetosphere generates electric fields and currents in the high-latitude ionosphere, where energy from the solar wind is dissipated as heat. With moderately southward IMF, the total ionospheric heating in both hemispheres is several hundred gigawatts (GW) [*Chun et al.*, 1999, 2002; *McHarg et al.*, 2005], and during major geomagnetic storm periods the heating may exceed 1000 GW [*Lu et al.*, 1998]. The result is that the thermosphere expands upward, creating additional drag on objects in low Earth orbit (LEO). This variability of drag forces causes difficulties for tracking and predicting the trajectories of thousands of space objects [*Wright*, 2007]. There have been instances when International Space Station crew members have needed to take emergency actions because of the risk of collisions with debris, as occurred on both 12 March 2009 and 1 December 2009.

[3] In 2009, the Iridium 33 communication satellite was destroyed by collision with a nonoperational satellite (Cosmos 2251), appreciably increasing the debris in Earth's orbit [*Burke et al.*, 2010]. The proliferation of space debris results in a requirement for improved capabilities for predicting the state of the thermosphere at any given time.

[4] In the absence of geomagnetic storms, the dominant heating of the thermosphere is due to the flux of solar, extreme ultraviolet (EUV) radiation [*Tobiska et al.*, 2008]. During magnetic storms, the primary component of energy flow that causes thermospheric expansion is the Poynting flux associated with the high-latitude electric fields and currents. This energy is dissipated in the ionosphere as both Joule and frictional heating and is transferred to the neutral atmosphere. The electric fields and currents that transmit the energy are in turn driven by the solar wind and interplanetary magnetic field (IMF) originating from the sun. Another source of energy is in the kinetic energy of the precipitating auroral particles. During disturbed periods, the Joule heating is a larger source of energy than particle precipitation [*Richmond et al.*, 1990; *Lu et al.*, 1995; *Anderson et al.*, 1998;

[1]National Institute of Aerospace, Virginia Polytechnic Institute and State University, Blacksburg, Virginia, USA.
[2]Air Force Space Command, Peterson AFB, Colorado Springs, Colorado, USA.
[3]Air Force Research Laboratory, Hanscom AFB, Bedford, Massachusetts, USA.
[4]Space Environment Technologies, Pacific Palisades, California, USA.

0148-0227/11/2010JA015685

Emery et al., 1999; *Knipp et al.*, 2004]. More recently, *Lu et al.* [2010, pp. 5–6] found the following:

> Joule heating is the dominant form of magnetospheric energy input into the thermosphere and is about two to three times larger than auroral energy input during active times. Auroral power is also closely correlated with Joule heating, with a correlation coefficient of 0.82.

[5] Solar radiation, auroral particle precipitation, and Joule heating also affect the chemistry of the thermosphere, most notably by enhancing the level of nitric oxide (NO) in the lower thermosphere. It is known that NO is an efficient radiative cooler for the thermosphere [*Sharma et al.*, 1996; *Duff et al.*, 2003], and it has been postulated that this radiative cooling acts as a "natural thermostat" in mitigating the effects of intense solar disturbances on the atmosphere [*Mlynczak et al.*, 2005]. The reaction between atomic nitrogen and molecular oxygen that produces NO is strongly dependent on temperature [*Bailey et al.*, 2002]. Solar soft X-ray irradiance is the primary energy driver for producing NO at low latitudes [*Barth et al.*, 1988]. At high latitudes, auroral electrons are considered to be the primary source of energy that leads to enhanced NO production [*Siskind et al.*, 1989; *Sætre et al.*, 2007; *Barth et al.*, 2003]. More recently, there has been a greater appreciation for the role of high-latitude Joule heating in NO production, primarily because the production rates are so sensitive to the temperature [*Barth et al.*, 2009; *Barth*, 2010]. *Barth* [2010, p. 1] states the following:

> During geomagnetic storms, gravity waves propagate from the polar regions toward the equator heating the thermosphere at 140 km and higher. These gravity waves are produced by Joule heating that occurs at latitudes of 60° and higher. The heating leads to an increase in the density of nitric oxide at 140 km in the thermosphere. On some occasions, the increased nitric oxide diffuses downward to the 110 km level causing the nitric oxide density at that level to increase substantially.

[6] *Lu et al.* [2010] have found a close correlation between global Joule heating power and global NO radiative cooling power. The importance of the relationships between NO production and the results presented here are discussed in section 4.

[7] Neutral density measurements on orbiting satellites have been used to analyze the changes in the thermosphere resulting from solar radiation, solar wind, and IMF energy transfer. These densities are derived from changes in orbital velocity obtained from accelerometers. Such instruments have been flown on the Challenging Minisatellite Payload (CHAMP) and Gravity Recovery and Climate Experiment (GRACE) satellites [*Tapley et al.*, 2004; *Bruinsma et al.*, 2004].

[8] *Schlegel et al.* [2005] reported unexpected detection of considerable structure in high-latitude thermospheric densities as derived from an accelerometer on board the CHAMP satellite. The amplitude of the density extrema can reach 50% over ambient, clustered around 75° geomagnetic latitude, while regions of lower density are near the poles.

[9] *Sutton et al.* [2005] reported the following observations from CHAMP measurements: During the first stage of geomagnetic activity on 29 October 2003, on the dayside elevated density levels of the order of 300% could be seen at northern latitudes. On the nightside density enhancements last longer than on the dayside and can be seen to travel toward the equator. In comparison, the dayside density enhancements exhibit much less dispersion to lower latitudes. There is a 3- to 6-hour delay between the onset of activity and equatorial response. In comparison with the NRL-MSISe00 empirical density model, during times of elevated magnetic activity, daytime density measurements are higher than modeled density by up to a factor of 2.

[10] In a later study using CHAMP measurements, *Sutton et al.* [2009, p. 1] reported that "generally, the response times are between 3 and 4 h at low latitudes while less than 2 h at midlatitudes to high latitudes." Their study used the Assimilative Mapping of Ionospheric Electrodynamics (AMIE) algorithm [*Richmond*, 1992] to calculate the Northern Hemisphere Joule heating index for comparison with the CHAMP measurements. A similar study by *Crowley et al.* [2010] observed conspicuous density enhancements in the dayside cusp region that resulted from unexpectedly large amounts of energy entering the ionosphere-thermosphere system during intervals of strong IMF.

[11] *Bruinsma et al.* [2006], using both CHAMP and GRACE accelerometer measurements, found global-scale increases in the thermospheric density on the order of 300% to 800% during a storm on 20–21 November 2003, with relatively little time delay at high latitudes and with about a 4-hour delay at the equator. There was an asymmetrical response at high latitude, with a greater density enhancement occurring in the summer Southern Hemisphere than in the north, which *Bruinsma et al.* [2006] attributed to a higher ionospheric conductivity and thereby a higher level of Joule heating.

[12] *Burke et al.* [2007] also found an ~4-hour delay between an enhancement in the magnetospheric electric field, derived from interplanetary parameters, and proportional density enhancements observed using GRACE, using whole orbit averages. Density increases were found to be highly correlated with the *Dst* index, and during the recovery phase the thermosphere relaxed more quickly than *Dst*. It had been found that models of the thermosphere available at the time underpredicted storm time density increases by over 100% and that local densities varied widely but that orbit averaged evolved systematically.

[13] In general, prior studies have mainly provided qualitative descriptions of the thermosphere's evolution during geomagnetic storms, rather than providing a quantitative study of the changes in thermospheric energy content, temperature, and density profiles compared with the energy deposited into the system. One way to quantify the energy input is with statistical models that map the high-latitude electric fields and currents as a function of the solar wind and IMF.

[14] One such empirical model is described by *Weimer* [2005a] and referenced hereafter as W05. This model is derived from measurements of both the electric and magnetic fields on the Dynamics Explorer-2 satellite and can produce maps for both the electric potential and field-aligned current (FAC) patterns. Magnetic Euler potentials are used as the basis for the FAC model, and this model can also calculate the magnetic perturbations associated with the currents. The two potential mappings are used together to calculate the Poynting flux and resulting ionospheric heating as a function of time, using a given time series of solar wind/

IMF measurements [*Weimer*, 2005b]. The primary advantage that the W05 model has over other methods, including some numerical models, is that it does not depend on any models or assumptions about the ionospheric conductivity. The conductivity variations as a function of location, season, and IMF are implicitly contained in the FAC model.

[15] *Codrescu et al.* [1995] had proposed that, since empirical models lack spiky electric fields at small spatial scales, such models are not able to accurately calculate the total polar Joule heating. It is generally thought that the lack of small-scale "electric field variability" will result in a considerable underprediction of total energy dissipation [*Matsuo et al.*, 2003; *Johnson and Heelis*, 2005; *Matsuo and Richmond*, 2008; *Deng et al.*, 2008]. The majority of such studies are theoretical and often use numerical simulations. Most ignore the effects of variable conductivity. *Cosgrove et al.* [2009] found that an anticorrelation between spatial fluctuations in conductance and squared electric field may partially compensate for the effects of the field variability.

[16] A quantitative test of ionospheric heating computed with the W05 model was reported by *Wilson et al.* [2006], who compared the model's calculations with observations of neutral density distributions derived from 6 months of measurements from the Air Force High Accuracy Satellite Drag Model (HASDM). HASDM was developed by the Air Force to improve their satellite orbit prediction capability [*Storz et al.*, 2002]. The Dynamic Calibration Atmosphere (DCA) portion of the model [*Casali and Barker*, 2002] is based on a near real-time correction to the Jacchia density model [*Jacchia*, 1970]. Tracking data from 75 to 80 calibration satellites is used to produce a new global density distribution every 3 hours. HASDM does not have sufficient spatial resolution to discern features such as the auroral zone, but it does accurately determine global thermospheric changes.

[17] For the comparison with the W05 model heating, *Wilson et al.* [2006] derived a quantity called ΔTPE_{200}, which is the change in gravitational potential energy for the thermosphere above 200 km altitude. This quantity is obtained from the HASDM output by integrating the product of the change in mass density as a function of position and the gravitational potential. This integral includes the spherical volume that starts at an altitude of 200 km, the lower limit of reliable HASDM output, and extends to infinity. Although the majority of the heating in storms is deposited in the ionosphere at lower altitudes, most of this heat goes into raising the temperature of the neutrals in the thermosphere and working to expand their mass upward against the force of gravity.

[18] On day to week timescales during periods without geomagnetic storms, it was determined that there is an excellent correlation between the solar EUV energy flux and ΔTPE_{200}. During the shorter storm periods, there were obvious changes in ΔTPE_{200} where the energy from auroral Joule heating and particle flux were the primary contribution. The total Joule heating was found to be larger than the energy from precipitating auroral particles, with ratios ranging from 1.7 to 6.9. For events with $\Delta TPE_{200} \geq 2.5 \times 10^{15}$ J, the average ratio is 3.2. Together these two sources supplied several times the energy needed to account for the change seen in ΔTPE_{200}.

[19] *Wilson et al.* [2006] fit the ΔTPE_{200} curves with a simple differential equation as a means to compare the energy inputs with the changes in total energy and also to account for losses due to a gradual exponential cooling. *Burke* [2008] and *Burke et al.* [2009] further developed this concept that the thermosphere acts as a "driven-dissipative thermodynamic system," showing that a powerful method for modeling the time evolution of the thermosphere is to simply keep track of the total energy budget of heat going in versus cooling losses. This new method is based on an analysis of the thermospheric model of *Jacchia* [1977] (J77). The J77 model consists of a set of density and temperature profiles, each uniquely specified by an exospheric temperature T_∞. In following up on the method used by *Wilson et al.* [2006], *Burke* [2008] used an analysis of the J77 tables to calculate the total volume-integrated gravitational potential energy of the thermosphere above an altitude of 100 km, as well as adding in the smaller amount thermal energy. They found that this total energy is linearly related to the average exospheric temperature by

$$E_{th}(J) = 5.365 \cdot 10^{17} + 8.727 \cdot 10^{13} \bar{T}_\infty \quad (1)$$

where E_{th} is the total energy of the thermosphere above 100 km in Joules. $\bar{T}_\infty$ is the globally averaged exospheric temperature in degrees Kelvin, preceded by the linear scaling factor that converts this temperature to total energy. Analysis of the J77 tables also indicated that

$$\bar{T}_\infty \approx 1.155 T_{\infty\,\mathrm{min}} \quad (2)$$

where $T_{\infty\ \mathrm{min}}$ is the "global nighttime minimum exospheric temperature." A concise summary of these results is provided by *Burke et al.* [2010]. Models of the thermosphere other than J77 may produce different results.

[20] *Burke* [2007] modeled the variability of the component of E_{th} due to the energy from the solar wind with a differential equation that used a reformulation of the Volland-Stern electric field to obtain the total energy input. τ_E = 6.5 hours was used for the relaxation time of the thermosphere cooling rate.

[21] Recently, *Bowman et al.* [2008a] developed a new density model that uses the *Jacchia* [1970] model as the basis for the diffusion equations. New exospheric temperature and semiannual density equations are employed to represent the major thermospheric density variations. This model, named Jacchia-Bowman 2008 (JB2008), uses a new set of solar indices to represent the total solar energy flux. It is an updated version of a prior model by *Bowman et al.* [2006, 2008b]. In addition to the $F_{10.7}$ index for radio flux, JB2008 and its predecessor use EUV flux from SOHO and solar middle ultraviolet (MUV) flux from NOAA satellites [*Tobiska et al.*, 2008]. These new solar indices are used to replace Jacchia's earlier derivations for the global nighttime minimum exospheric temperature. *Bowman et al.* [2008a] used the notational abbreviation T_c rather than $T_{\infty\ \mathrm{min}}$ to represent this exospheric temperature, and this T_c notation is used in the remainder of this paper. All other calculations within the JB2008 model use the derived T_c to obtain density as a function of location, day of year, and time of day.

[22] In JB2008, T_c is calculated from

$$T_c = 392.4 + 3.227\bar{F}_S + 0.298\Delta F_{10} + 2.259\Delta S_{10} + 0.312\Delta M_{10} + 0.178\Delta Y_{10} \quad (3)$$

The delta values represent the difference of the daily and 81-day centered, boxcar average value of each index, where F_{10} represents the standard, 10.7-cm solar radio flux, S_{10} represents EUV flux from SOHO, M_{10} is obtained from MUV flux from NOAA satellites, and Y_{10} uses solar X-ray emissions measured on the GOES satellite [*Tobiska et al.*, 2008]. $\bar{F}_S$ is obtained from a weighted combination of the running-average values of F_{10} and S_{10}.

[23] JB2008 additionally handles geomagnetic storm periods by incorporation of an equation by *Burke* [2008] that describes the exospheric temperature response as a differential equation using the *Dst* index and further modifications depending on *Dst* storm minimum. The "geomagnetic storm index" used by JB2008 is the exospheric temperature change as calculated from *Dst* indices by a separate, external utility program. *Bowman et al.* [2008a, p. 18] reported that during major storm periods, the error reduction obtained "is from over 60% for Jacchia 70 and over 35% for NRLMSIS, to 16% for JB2008."

[24] It is desirable to reduce the errors during major geomagnetic storms even further, as it would enhance the ability to track satellites and orbital debris following such storms. This paper presents one method to accomplish this objective on the basis of empirical models of the energy dissipated at auroral latitudes.

2. The Auroral Poynting Flux Model

[25] The W05 model maps the electric potential and magnetic Euler potentials above the ionosphere as a function of the solar wind and IMF. The electric field is obtained from the gradient of the electric potential, and the gradient of the magnetic Euler potential, with a 90 degree rotation, produces the magnetic perturbation above the ionosphere that is caused by the FACs. The cross product of these two vector fields produces the Poynting flux into the polar ionosphere [*Weimer*, 2005b], where most of the energy is dissipated as heat [*Deng et al.*, 2008]. The Poynting flux is generally highest in the auroral zones, although there are also significant amounts poleward in the open field line region known as the polar cap. As pointed out by *Vasyliunas and Song* [2005, p. 8] and *Song et al.* [2005, paragraph 1], "the coupling of ionosphere and neutral atmosphere is better described as a (frictional) neutral drag process rather than as Ohmic dissipation." All uses of the term "Joule heating" in this paper implicitly refer to the total heat dissipated by both processes.

[26] The most recent version of the model [*Weimer*, 2005a] uses Spherical Cap Harmonic Analysis (SCHA) functions [*Haines*, 1985] to calculate the potential functions within a spherical cap that expands and contracts with variations in the IMF. Both potential functions within the spherical cap are described by the equation

$$\psi(\lambda,\phi) = \sum_{k=0}^{12}\sum_{m=0}^{2<k} P^m_{n_k(m)}(\cos\lambda)\left(g^m_k \cos m\phi + h^m_k \sin m\phi\right) \quad (4)$$

The angle λ is the colatitude. $P^m_{n_k(m)}$ is an Associated Legendre function with integer order m and real noninteger degree n. As described by *Haines* [1985], the real value of the degree n is a function of both the integers k and m, hence the notation $n_k(m)$. The values of n also depend on the "polar cap half angle λ_o," which is the colatitude of the variable low-latitude boundary. The values of n change as this boundary expands and contracts as a function of the IMF. The harmonic coefficients g^m_k and h^m_k for each term in the series are calculated within the W05 model as functions of solar wind and IMF parameters, as well as dipole tilt angle.

[27] In the results presented here, the interplanetary space environment measurements are from NASA's Advanced Composition Explorer (ACE), using data obtained by the Magnetic Field Instrument [*Smith et al.*, 1998] and the Solar Wind Electron, Proton, and Alpha Monitor (SWEPAM) [*McComas et al.*, 1998] instruments. The "Level 2" data are used, having a cadence of 16s and a starting date in early February 1998 and available from online archives maintained by NASA. These measurements, taken at an orbital position at approximately $240R_E$ "upstream" from the Earth, are propagated to the nose of the bow shock using a technique that accounts for variations in the orientation of the planes of constant phase [*Weimer and King*, 2008]. An average offset position at X = $14.6R_E$ GSE [*Fairfield*, 1971] was used for the position of the bow shock. The propagation time delays are on the order of 1 hour. An additional delay is added before computing the potentials in the ionosphere.

[28] *Weimer et al.* [2010] used the same IMF propagated data set to compare with geomagnetic variations measured at multiple ground-level magnetometers. Correlations with auroral zone magnetometers were found to be highest when using an AE-like compilation with a 5 min resolution, and IMF parameters averaged over a time period of 20–25 min. The correlation peaks at delays of 30–35 min from bow shock to ionosphere as measured from the centers of the IMF averages. In the results presented in this study, the W05 model calculations of the auroral heating are calculated from 20 min IMF averages over time periods starting at 40 m and ending at 20 m before each W05 calculation. The total heating in each hemisphere is calculated at every 4 min in the years 2002–2006. The calculations for the Southern Hemisphere use the same IMF parameters as in the Northern Hemisphere, except that the sign of the y-component of the IMF is reversed. W05 has seasonal variation that is determined by the "dipole tilt angle," which is the complement of the angle between the magnetic dipole axis and the Earth-Sun line and used in the rotation between the SM and GSM coordinate systems. A sign reversal is also used on the dipole tilt angle for the Southern Hemisphere calculations.

[29] There is one interval where the original Level 2 data could not be used for the ACE plasma measurements. During the famous "Halloween storm" [*Gopalswamy et al.*, 2005], the solar emissions so overwhelmed the plasma instrumentation on the ACE spacecraft that normal Level 2 data processing could not provide valid measurements of solar wind velocity and density. With special handling of this event, R. M. Skoug at Los Alamos National Laboratory provided revised solar wind velocity and density values

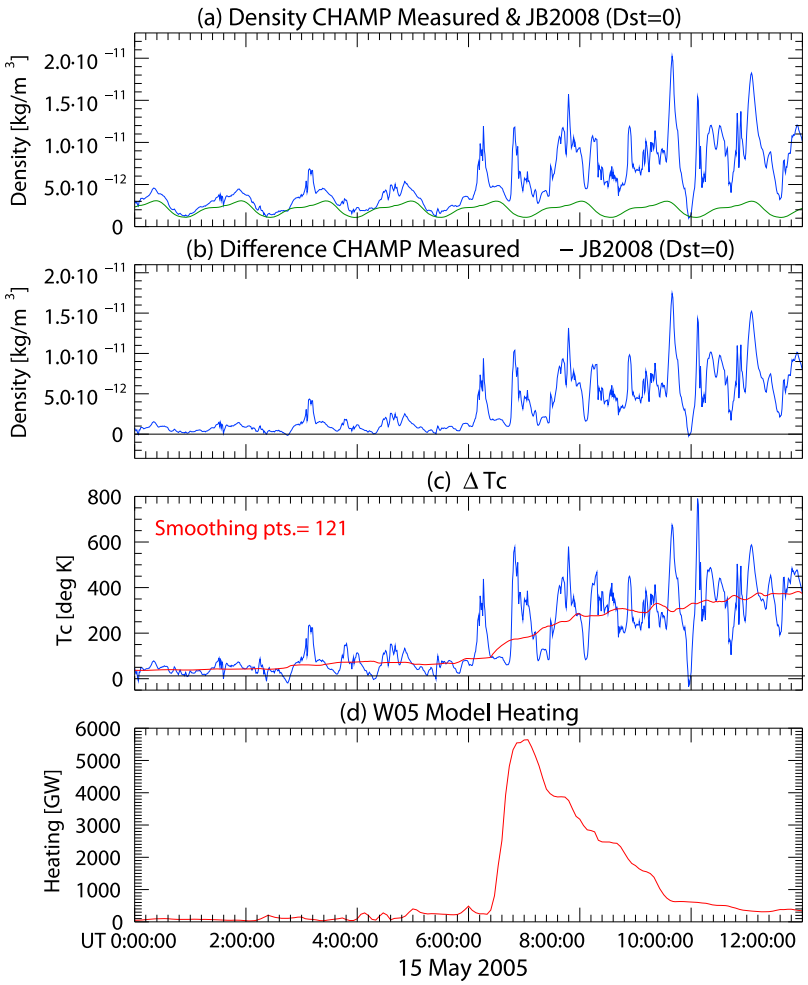

Figure 1. Comparison of CHAMP measurements with JB2008 model and total polar heating from W05 model at 0000–1200 UT on 15 May 2005. (a) The blue line shows the density values derived from accelerometer drag measurements, and the green line indicates the density from the JB2008 model at the satellite locations/altitude. (b) The difference between the measured and modeled densities. (c) The blue line shows the temperature correction in degrees Kelvin that results in a JB2008 calculation that exactly matches the measured densities. The superposed red line shows the same temperature after smoothing with a 121-point boxcar average. (d) The red line shows the total heating in the Northern and Southern hemispheres as calculated from the IMF using the W05 model.

[*Skoug et al.*, 2004] that for this study have been merged with the Level 2 measurements.

3. Thermosphere Density/Temperature Measurements

[30] Measurements of atmospheric density at thermosphere altitudes obtained from accelerometers on both the CHAMP and GRACE-A satellites are used for developing and testing the prediction methods presented here. Although there are two GRACE satellites, only data from the "A" satellite are used. GRACE-B followed GRACE-A very closely in the same orbit. Converting the accelerometer-derived drag measurements into density values is a difficult task, and there exist several different versions of the converted data at different institutions. The data used in this study are from a database maintained at the University of Colorado [*Sutton et al.*, 2007] that is easily accessible over the Internet. Version 2.2 of the density calibrations is used.

[31] The JB2008 thermosphere model is used extensively for the comparisons of the ionospheric heating with the satellite density measurements. Figures 1 and 2 show an example of a comparison at a relatively high time resolution, where both CHAMP and GRACE measurements are shown with W05 calculations of polar heating during a time period that had a sudden increase in the heating rate. The graphs in Figures 1a and 2a show the density values obtained by the satellite drag measurements using the blue lines. In the Colorado database, bin-averaged values are provided at every three degrees of geographic latitude. For comparison to the measurements, the green lines show the density from the JB2008 model at the satellite location/altitude when the *Dst*-derived correction to T_c is always set to zero, so that only the solar indices are used to calculate T_c. Figures 1b and 2b show the difference between the measured densi-

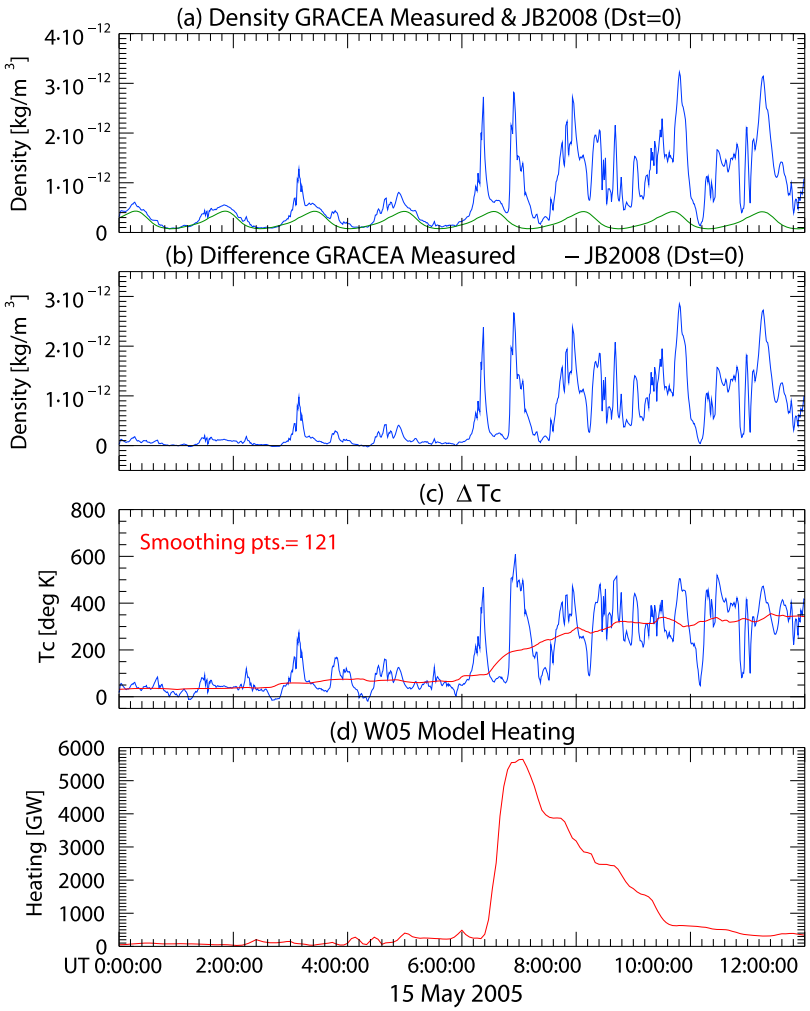

Figure 2. Comparison of GRACE-A measurements with JB2008 model and total polar heating from W05 model at 0000–1200 UT on 15 May 2005. The format is the same as in Figure 1.

ties and the JB2008 model results, again using a blue line in each. As CHAMP orbits at a lower altitude than GRACE, the density values and differences shown in Figure 1 are approximately an order of magnitude higher than the corresponding values shown in Figure 2.

[32] For reference, Figures 1d and 2d use a red line to show the total heating in the Northern and Southern hemispheres as calculated from the IMF using the W05 model at 4 min increments. It is evident that after 0600 UT on 15 May 2005, the heating jumped from a relatively low level to several thousand gigawatts (GW) in only 1 hour. During the first two orbits shown in these graphs, the agreements between the measured density and the JB2008 model's values are good; after the heating increases, the measured and model values obviously start to diverge, as the *Dst* corrections for T_c in JB2008 are not being used (set to zero) in the comparisons shown.

[33] Figures 1c and 2c use blue lines to show the values of the correction to T_c, in degrees Kelvin, that results in a JB2008 calculation that exactly matches the measured densities. This correction is referred to here as ΔT_c. As T_c represents the "global nighttime minimum exospheric temperature," changes in this global average obviously cannot occur as quickly as indicated with these ΔT_c values. On very short timescales, ΔT_c can be considered a proxy index for how far the local exospheric temperature at the location of the satellite has been perturbed from the global average. Nevertheless, the ΔT_c values at CHAMP and GRACE are in good agreement, with some differences due to their different orbits. Their differences are mostly removed when the ΔT_c values are smoothed with a 121-point boxcar average, corresponding to approximately one complete orbit, as shown with the superposed red lines in 1c and 2c. These ΔT_c values are a convenient way to compare the measurements from the different satellites, as well as an effective way to gauge the influence that the auroral heating has on the thermospheric temperatures.

[34] Upon close examination of the averaged ΔT_c values obtained from CHAMP and GRACE, it was noticed that the values from CHAMP tended to be slightly higher than those from GRACE. Using a linear equation to compare the two,

$$\Delta T_{c\,\mathrm{CHAMP}} = a\ \Delta T_{c\,\mathrm{GRACE}} + b \tag{5}$$

a least-error fit with 1 year's data was used to obtain the values of a and b. The top section in Table 1 shows the

Table 1. Comparing ΔT_c Results From CHAMP and GRACE[a]

Year	a	b(°K)	Corr.
	Initial Results		
2003	1.017	21.2	0.971
2004	1.065	12.5	0.966
2005	1.099	10.3	0.970
2006	1.104	−4.0	0.947
	Adjusted Results		
2003	0.989	5.9	0.973
2004	1.021	0.2	0.965
2005	1.059	−1.1	0.970
2006	1.017	−12.2	0.922

[a]Top section shows the initial a and b coefficients resulting from a least-error fit with equation (5). The linear Pearson correlation coefficients are in the last column. Bottom section shows the same results after slight adjustments were made to the original CHAMP and GRACE density values, which made a closer to 1.0, and in all years except 2006 reduced the offsets b.

results of the fit for the years 2003 through 2006, as well as their correlation coefficients. There are gaps spanning about 30 days in 2006. The results show that the CHAMP values tended to be higher than those from GRACE by about 2% to 10%, plus a constant offset ranging from −4 to 21°K. There is a common trend in all 4 years, possibly the result of minuscule satellite weight/orientation changes. It is much more likely that the JB2008 calculations at the different altitudes are affected by the declining solar EUV flux in the decreasing solar cycle toward anomalously low levels in 2007–2009 [*Solomon et al.*, 2010].

[35] Not knowing which satellites' ΔT_c results could be more correct than the others, it was decided to use a neutral approach whereby the original density measurements in both data sets were adjusted slightly to bring the ΔT_c results into better agreement. Although the scaling factors seemed to vary by year, the same adjustments were used for all years, where the CHAMP densities were multiplied by 0.96 and the GRACE densities were multiplied by 1.04. Following a new derivation of the orbit-averaged ΔT_c values, another comparison yielded the results shown in the bottom half of Table 1. Following the density adjustments, the ratios of the ΔT_c values are to within 6% in all years and to within 1% in 2003, and the offsets were less than 6°K, except in 2006. That the offsets were reduced simply by multiplying the densities seems counterintuitive, but apparently is the result of the highly nonlinear density changes as a function of altitude in the thermosphere. Note that these results apply only to version 2.2 of the Colorado density database, and different acceleration-to-density calculations are used at other institutions. These results are also model-dependent, as JB2008 is used to derive ΔT_c values.

4. Derivation of ΔT_c From Auroral Heating

[36] Following upon the methods used by *Burke* [2008] and *Wilson et al.* [2006], the total auroral heating from the W05 model is used to calculate ΔT_c values as a function of time, employing a differential equation that increases the temperature in proportion to the heating energy input and decreasing the temperature with an exponential cooling. In numerical form, the temperature at time step $n + 1$ is derived from that at the prior step by

$$\Delta T_c(t_{n+1}) = \Delta T_c(t_n)\left(1 - {}^{\Delta t}/_{\tau_c}\right) + \beta H_J \Delta t \qquad (6)$$

where H_J is the total heating from the W05 model in both hemispheres and β is a scaling factor that relates the temperature increases to the heat input in each time step. This method uses the findings by *Burke* [2008] that the global average temperature of the thermosphere scales linearly with its total thermal energy. The exponential cooling rate of the thermosphere is τ_c.

[37] By reiterative comparisons of the results from equation (6) with the "measured" ΔT_c derived from CHAMP and GRACE data, the optimal values of β and τ_c are obtained. The values that produced the best fits could vary from case to case, depending on which time periods or satellites are used. The results indicated that one fixed value for τ_c would not work equally well for all cases. The events with very large thermosphere temperature increases (400°K or more) cooled or decayed at a much faster rate (smaller τ_c) than in time periods having less heating, with cooling time constants ranging from 5 to 14 hours. Better agreement in a wider range of events was obtained by changing the cooling rate of the thermosphere in proportion the heating during a prior interval. As discussed in the Introduction, particle precipitation and Joule heating act to increase the amount of NO in the thermosphere. This extra NO then acts as an efficient radiative cooler for the thermosphere, acting as a natural thermostat [*Mlynczak et al.*, 2005].

[38] To account for the cooling effects of NO in a simple manner, a variable cooling rate was introduced whereby τ_c would decrease in proportion to a variable representing an enhancement in the level of NO:

$$\tau_c = \tau_0 - \eta \Delta NO \qquad (7)$$

[39] The amount of the NO enhancement is increased in proportion to the Joule heating and then decays exponentially when production ceases. Enhancement of NO by particle precipitation is assumed to be in proportion to that due to the heating. A numerical equation identical to equation (6) is used for the variable representing the relative change in the level of NO:

$$\Delta NO(t_{n+1}) = \Delta NO(t_n)\left(1 - {}^{\Delta t}/_{\tau_{NO}}\right) + \gamma H_J \Delta t \qquad (8)$$

[40] The variable representing the increased NO has a scaling that is entirely arbitrary, so that γ is simply set to 0.0001 per GW of heating when the time step is 4 min. This value of γ results in a ΔNO that ranges between 0 and 50 on the arbitrary scale and η scales in proportion. Values for the variables in equations (6) through (8) were derived using the total heating as a function of time and the ΔT_c derived from both the CHAMP and GRACE measurements. All data from the years 2003 through 2005 were used in a reiterative least-error fit. A modified downhill simplex method (also known as "Amoeba") [*Press et al.*, 1986] was employed to find the variables that minimized the total square error. The data in the years 2002 and 2006 were not used in this fit, in order to

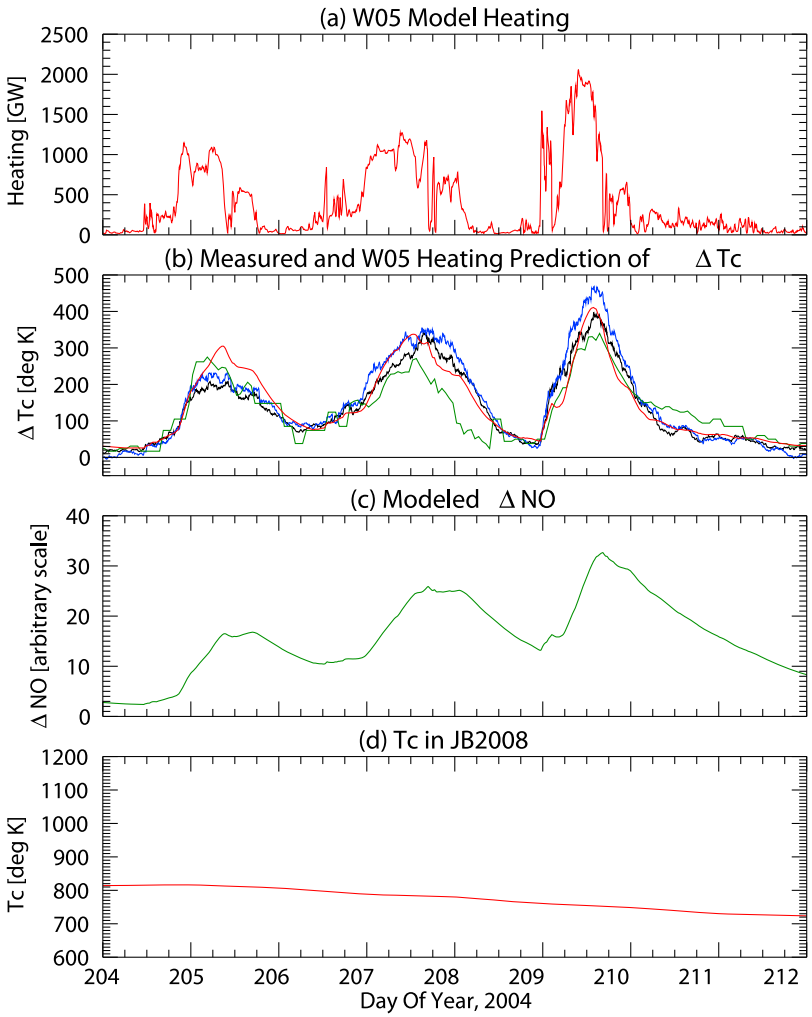

Figure 3. Thermosphere temperature changes derived from W05 model compared to CHAMP and GRACE measurements on days 204–212 in 2004. (a) Red line shows the total heating from W05 model with a saturation correction applied. (b) Red line shows thermosphere temperature changes derived from the W05 model in the form of a correction ΔT_c for the JB2008 model. The superposed black and blue lines show the values of this ΔT_c correction that are derived from CHAMP and GRACE drag measurements. For comparison, the green line shows the ΔT_c correction that is derived from the *Dst* index as currently used in the JB2008 model. (c) The level of a variable that represents changes in the amount of nitric oxide (NO) in the thermosphere, which is used to calculate the cooling rate of ΔT_c. (d) The background level of thermospheric temperature that JB2008 uses as derived from solar indices.

be used afterward for validation. The variables that produced the best overall results were $\beta = 0.00276$°K/GW, $\tau_0 =$ 14.6 hours, $\eta = 0.281$ hours/unit, and $\tau_{NO} = 28.0$ hours. The values of β and η depend on the time step, which is 4 min.

[41] An example of how the calculation of the ΔT_c temperature correction compares with measurements is shown in Figure 3, from days 204 to 212 (22 to 30 July) in 2004. The total heating used in the calculation is shown as the red line in Figure 3a. ΔT_c calculated using equations (6) through (8) is shown as the red line in Figure 3b. For comparison, the blue and black lines in Figure 3b show the ΔT_c values derived from CHAMP and GRACE, respectively, using the whole-orbit moving averages. The value of ΔT_c in the numerical calculation in equation (6) was initialized at the first time step at the start of the year. The green line in Figure 3b shows the values of the ΔT_c correction derived from the *Dst* index that is presently used in the JB2008 model. It does remarkably well in all cases, considering that only the *Dst* index is used. For reference, Figure 3c shows the level of the ΔNO enhancement on our arbitrary scale, as calculated with equation (8). This example shows how the decay rate of ΔT_c becomes faster (smaller time constant) as the heating increases. At the point where the ΔNO reaches a peak level of 33, the cooling time constant is reduced from 14.6 h to 5.33 h. The graph in Figure 3d shows the background level of the global thermospheric temperature T_c that is used within the JB2008 program as calculated from the solar indices with equation (3), so that it can be seen how the corrections compare to the overall level.

[42] It was initially determined that, during time periods with high levels of solar wind driving, the optimal values of β were smaller than those obtained when the heating was

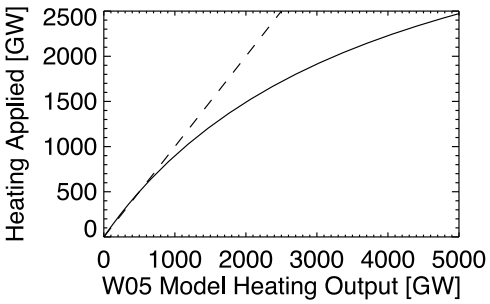

Figure 4. Saturation adjustment applied to W05 model outputs. Horizontal axis shows total heating from W05 model, and curve shows compensated output used for temperature calculations.

lower. This indicated that at the higher levels of driving, the W05 model is producing total heating levels that are too high. A nonlinear correction was applied to the Poynting flux totals to obtain good fits between the predicted and measured values of ΔT_c under a wide range of driving conditions.

[43] It is known that the electric potentials in the polar cap exhibit a saturation effect when the z-component of the IMF becomes increasingly negative [*Hill et al.*, 1976; *Siscoe et al.*, 2002]. This saturation curve has been investigated extensively through observations and theory, as reviewed by *Shepherd* [2007], and it may explain why the nonlinear correction is required. Another possible explanation is in the findings by *Deng et al.* [2008, p.2], from a numerical model, that "the thermosphere and ionosphere do not necessary respond in a linear fashion to the high-latitude energy inputs."

[44] Although the W05 model already had some saturation applied internally, it is possible that it is not enough, particularly since the satellite database does not contain many cases having an IMF magnitude over 15 nT. The results obtained here were derived by applying an additional saturation curve to the total heating levels using the curve shown in Figure 4. This curve is set so that the input and output levels are exactly the same at 500 GW. This reduction in the heating level was done separately for both the Northern and Southern hemispheres before adding them together. The heating rates shown in Figure 3 and later use this saturation adjustment, whereas the heating rates shown in Figures 1 and 2 are the original values from the W05 model.

[45] Additional examples are shown in Figures 5–7, all having the same format as Figure 3. Figure 5 covers days 311 to 318 (6 to 13 November) in 2004. Figure 6 covers days 296 to 328 (23 October to 24 November), showing an instance where the comparison is at its worst. This time period includes the "Halloween Storm" event, during which there was some uncertainty in solar wind and IMF data. For most of the time period shown in Figure 6, the agreement between measured and predicted values is to within 10° to 5° or less, with the exception of a period from days 300 to 308 during the peak of the storm. One possible explanation for the disagreement in this period is that the background level of T_c (shown in Figure 6d) could be too high. If the T_c that is derived by JB2008 from the solar indices is too large, then it will result in a derivation of the ΔT_c correction for the auroral heating that is too low or even negative. The agreement between the measured and predicted ΔT_c values is better in the later storm period on days 324–326, where the lower T_c level may be more accurate. Another possible explanation for negative ΔT_c values is that the accelerated thermospheric cooling caused by the extra NO production could be so efficient that the temperature drops below the expected model values. There are other time periods just following major heating events (not shown) where the measured ΔT_c corrections are also negative. The last example in Figure 7 shows the comparison for a longer time period, days 90 through 275 in 2005. The variations in the background level of T_c at the solar rotation period are evident in Figure 7d.

[46] Numerical measurements of the correspondence between the ΔT_c derived from the W05 model and the values derived from drag measurements are contained in Table 2. The average errors, standard deviations, and correlation coefficients for both CHAMP and GRACE comparisons are shown for the time periods graphed in Figures 3, 5, 6, and 7, as well as all of years 2002 through 2006. Only part of 2002 is used because of incomplete GRACE data in this year and some apparent mismatches between the JB2008 model and drag measurements earlier in the year. The average error is the total, absolute value of the differences at every point (4 min cadence) divided by the number of points. In the all-year results (bottom five rows in Table 2), this error ranges from 9.7°K to 19.3°K. The largest error is 32.8°K during the extreme conditions in 2003. To put these errors in perspective, the ΔT_c values range between approximately 100 to 600°K, which is in addition to the background level of T_c due to solar EUV radiation, in the range of 600 to 1000°K. The standard deviations range from 13.9°K to 25.8°K, and the correlation coefficients range from 0.82 to 0.91. For comparison, Table 3 shows the results of the same calculations using the values of ΔT_c that are derived from the *Dst* index for the JB2008 model. In the all-year periods, the average error using *Dst* ranges from 16.2°K to 25.8°K, and the largest is 63°K. The correlation coefficients range from 0.74 to 0.83. For both methods of ΔT_c calculation, the correlations are lowest in the years 2002 and 2003. These years had more geomagnetic activity, more frequent ΔT_c measurements with negative values, and higher solar EUV radiation, which affect the baseline T_c values.

5. Discussion

[47] Figures 1 and 2 show high temporal resolution graphs comparing density measurements from the CHAMP and GRACE accelerometers with the JB2008 model calculations, as well as the simultaneous auroral heating from the W05 model. It is apparent that the density changes that are seen at the satellite altitudes occur very quickly in response to changes in the auroral heating. After a small increase in the heating after 0200 UT on 15 May 2005, the satellites show obvious increases on their next pass 1 hour later. After the heating greatly increases quite suddenly between 0630 and 0700 UT, the densities are enhanced by a factor of 4 or more in the entire orbits a half-hour later. Thus, the heating that occurs in the polar caps is affecting the global ther-

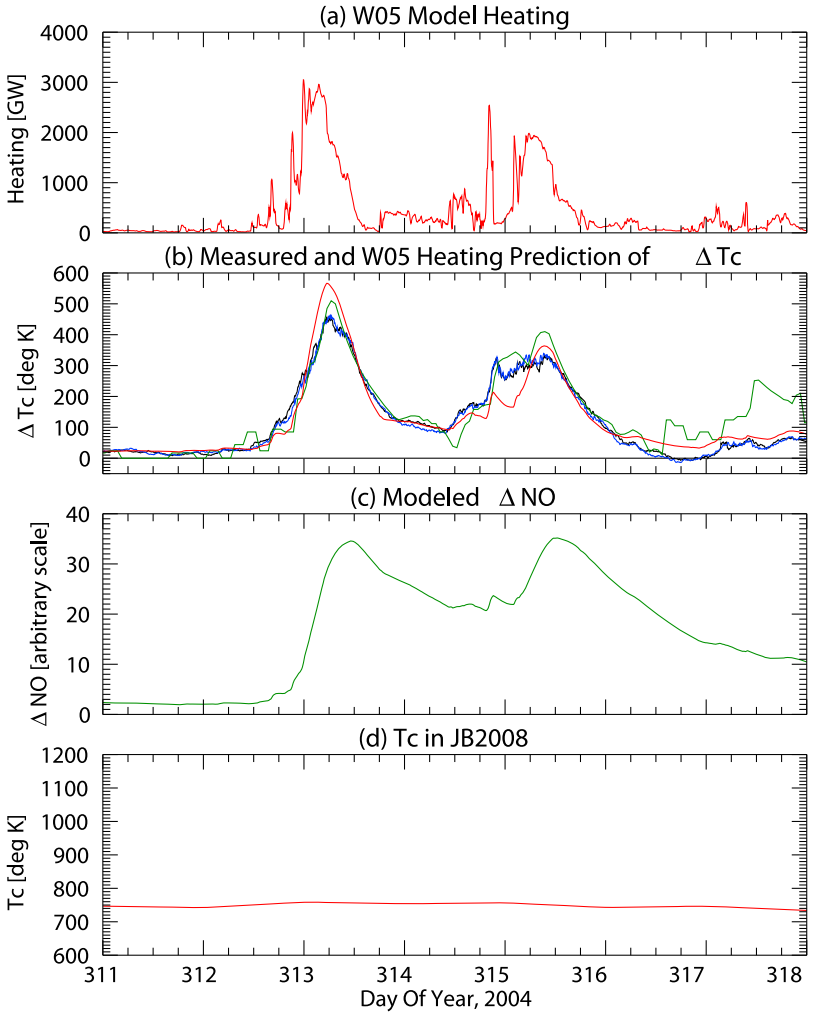

Figure 5. Thermosphere temperature changes derived from W05 model compared to CHAMP and GRACE measurements on days 311–318 in 2004. Format of the graph is the same as in Figure 3.

mosphere densities at all latitudes within a very short time period. The spiky nature of the density measurements might in part be due to [*Burke et al.*, 2007, p. 279] "encounters with strong head and tail thermospheric winds driven by anti-sunward convecting plasma." Nevertheless, the use of orbit averages effectively smooths out these spikes.

[48] The thermospheric density measurements have complex variations that result from changes in altitude, latitude, and solar illumination during each orbit. These changes make it difficult to compare measurements taken on different satellites or to quantify the overall state of the thermosphere. Comparing CHAMP and GRACE results is further complicated by their different altitudes, where there is normally an order of magnitude difference in densities. A technique is described in section 3 whereby aproxy for the temperature changes, ΔT_c, is calculated by use of the Jacchia equations within the JB2008 model. This appears to be a very useful method for quantifying the density changes in a way where they can be compared to each other and to simultaneous output from heating models. The ΔT_c results depend on the accuracy of both the JB2008 model and the underlying global temperature calculation using the solar indices. When the solar wind driving is at a very low level for 1 day or more, the ΔT_c values must drop to zero for this technique to work at all. That the near-zero ΔT_c values are frequently seen where they should be indicates that the JB2008 calculations, as well as T_c values derived from solar indices by *Tobiska et al.* [2008], are remarkably accurate in their comparison with the CHAMP and GRACE satellite density measurements.

[49] It is shown that the auroral heating calculated with the W05 model can be used in a simple differential equation to calculate the changes in the ΔT_c correction needed to calculate thermospheric densities using the JB2008 model. Comparisons with satellite drag measurements produce correlations in the range of 0.82 to 0.91. This correction from W05 can be used as a direct substitute for the *Dst*-derived correction that is presently used in JB2008. The test results shown in Tables 2 and 3 indicate that the results from the Poynting flux model have higher correlations with the average errors that are lower by approximately 5 to 10°K.

[50] As indicated by equations (1) and (2), taken from *Burke* [2008], raising T_c or $T_{\infty\ \mathrm{min}}$ by 1°K raises $\bar{T}_\infty$ by 1.155°K, increasing the total energy in the thermosphere above 100 km altitude by $1.01 \cdot 10^{14}$ J (as derived from the J77 model). Thus, the thermosphere can act as a giant

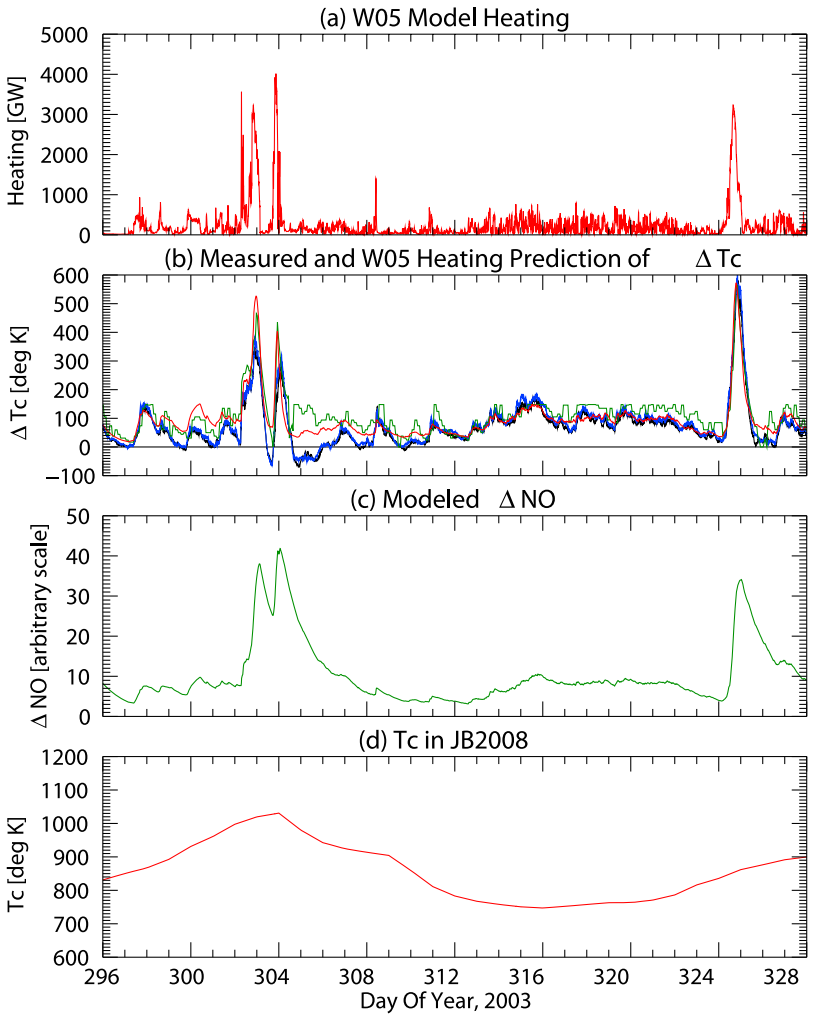

Figure 6. Thermosphere temperature changes derived from W05 model compared to CHAMP and GRACE measurements on days 296–328 in 2003. Format of the graph is the same as in Figure 3.

calorimeter, where a given change in the global average temperature is related to the total amount of thermal and potential energy that is contained in the system. This presents an opportunity to determine the accuracy of the total energy that is flowing into the ionosphere/thermosphere system as calculated by the W05 Poynting flux model.

[51] The automatic fitting routine had found that a value of 0.00276°K/GW for the β parameter in equation (6) produced the best fit with the CHAMP and GRACE measurements. This value for β corresponds to how much energy deposited in each time step is needed to match the temperature change in the thermosphere during the same time step. The temperature changes are derived from the differences between the CHAMP and GRACE density measurements and JB2008 model calculations, and all parts of this derivation have no knowledge about how the changes should relate to the total energy stored in the system. With a β equal to 0.00276°K/GW, an output of 362 GW from the W05 model over a period of 4 min (one time step) is needed to raise the T_c temperature by 1°K. A heat input of 362 GW during a 4 min interval amounts to $0.869 \cdot 10^{14}$ J, which is not much different from the $1.01 \cdot 10^{14}$ J obtained from J77. There is additional energy flowing into the system from the auroral particle precipitation, which *Wilson et al.* [2006] found to be a factor of 2 to 6 lower than the Joule heating. It can be concluded that with the addition of this particle energy, the W05 model is providing sufficient energy to account for the total change in energy in the thermosphere above 100 km. As mentioned before, the β factor was determined entirely by the automatic fitting routine rather than set in advance; the value required to match equations (1) and (2) was not even considered until after the fitting process had been completed. If the β that resulted from the fit was much smaller, then it would indicate that the W05 levels are too high, and if β was larger, it would indicate that the W05 Poynting flux totals are too low.

[52] In the Introduction, it was mentioned that several theoretical studies had concluded that since empirical models generally lack the variability in small-scale field structure, it is expected that empirical models will undercalculate the total Joule heating. As the W05 model is providing a very good match with the thermospheric temperature changes that are measured with CHAMP and GRACE, it appears that the effects of the small-scale variability are not so important. The most likely reasons are that the spiky fields could have a low duty cycle and also are

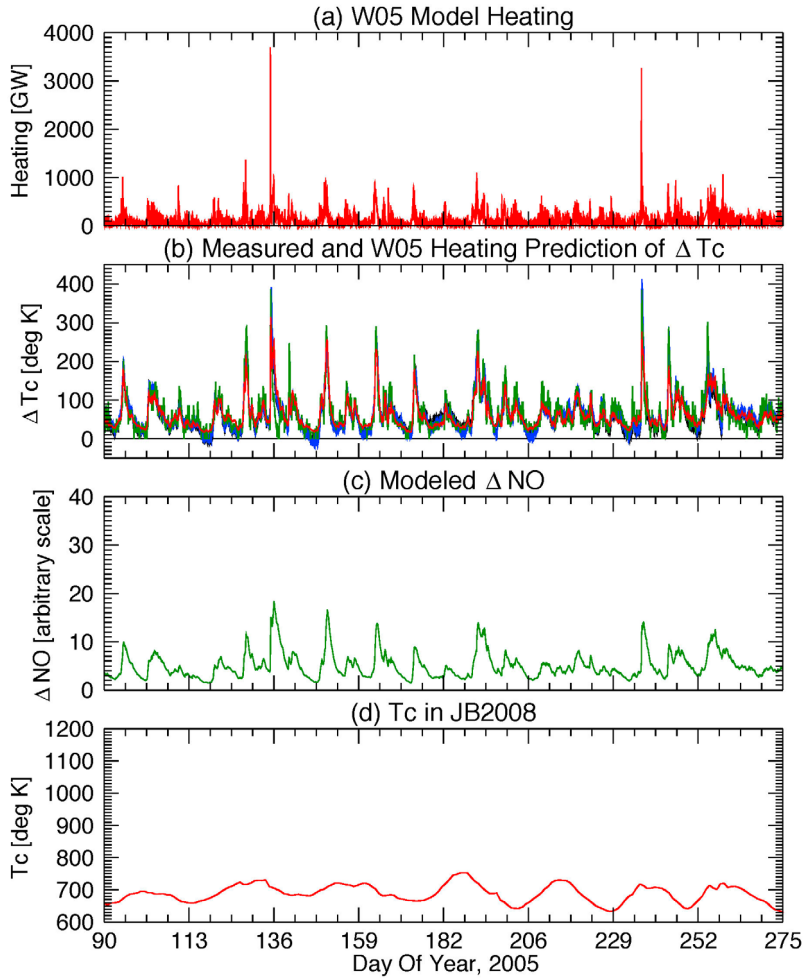

Figure 7. Thermosphere temperature changes derived from W05 model compared to CHAMP and GRACE measurements for days 90–275 in 2005. Format of the graph is the same as in Figure 3.

anticorrelated with conductivity enhancements. Regardless of whether the small-scale structure contributes appreciably to the total heating, apparently their contribution scales in proportion to the large-scale energy flow as would be expected from a turbulent energy cascade having a spectral power law. It was necessary to apply a reduction in the model output above the 500 GW level, as shown in Figure 3, which occurs when the IMF is southward at 15 nT. This indicates that the model output might actually be too high above this level.

[53] Within events having thermospheric temperature enhancements on the order of 400°K or more, the exponential cooling rates were always found to have time constants on the order of 5 to 6 hours, whereas during more quiescent time periods the cooling time constants were closer to 14 hours. The faster cooling rates (smaller time constant) are thought to be the result of additional NO that is produced as a by-product of the combined effects of auroral heating and particle precipitation; the extra NO then accelerates the cooling rate. The differential equations that predict the thermospheric temperature changes were modified to account for the variable cooling rates. This empirical modification serves as a measurement of how the decay rates change as a function of the prior levels of global heating. Physics-based calculations of NO production are not presently included in this formula.

[54] *Marsh et al.* [2004] used results from the Student Nitric Oxide Explorer (SNOE) satellite to construct an empirical, three-dimensional model of the NO concentration in the thermosphere, using empirical orthogonal functions

Table 2. Statistical Results of Comparison Between JB2008 Predictions and CHAMP and GRACE Measurements[a]

	Average Error (°K)		Standard Deviation (°K)		Correlation Coefficient	
Time Period	CHAMP	GRACE	CHAMP	GRACE	CHAMP	GRACE
2004 204–212	28.6	23.5	38.6	32.8	0.951	0.947
2004 311–318	27.8	27.4	39.3	38.7	0.950	0.950
2003 296–328	30.6	32.8	43.6	46.5	0.875	0.873
2005 090–275	12.4	11.5	17.4	15.2	0.943	0.942
2002 266–end	16.4	16.5	20.6	21.2	0.833	0.837
2003 All	19.3	17.7	25.8	24.6	0.819	0.816
2004 All	12.5	12.5	16.8	16.5	0.918	0.908
2005 All	15.5	12.4	20.6	16.7	0.898	0.912
2006 All	17.1	9.7	20.9	13.9	0.870	0.893

[a] ΔT_c used in JB2008 are from the W05 Poynting flux calculations, rather than the original values derived from the *Dst* index. First four rows correspond to the time periods shown in Figures 3, 5, 6, and 7.

Table 3. Statistical Results of Comparison Between JB2008 Predictions and CHAMP and GRACE Measurements[a]

Time Period		Average Error (°K)		Standard Deviation (°K)		Correlation Coefficient	
		CHAMP	GRACE	CHAMP	GRACE	CHAMP	GRACE
2004	204–212	46.9	36.7	63.0	48.9	0.879	0.871
2004	311–318	43.2	42.8	62.0	61.8	0.895	0.891
2003	296–328	41.4	46.4	54.9	59.3	0.850	0.849
2005	090–275	19.6	19.6	26.4	26.4	0.856	0.854
2002	266–end	25.0	25.8	32.5	34.8	0.771	0.775
2003	All	23.7	24.8	31.3	32.9	0.753	0.742
2004	All	19.4	18.4	26.3	25.2	0.818	0.831
2005	All	20.7	19.6	28.3	27.5	0.815	0.823
2006	All	21.1	16.2	26.7	21.9	0.778	0.796

[a]ΔT_c used in JB2008 are the original values, derived from the *Dst* index. First four rows correspond to the time periods shown in Figures 3, 5, 6, and 7.

(EOFs). They found a response of NO to auroral activity as measured with the planetary *Kp*, which supports the findings presented here. Additionally, there is a seasonal effect and a response to varying solar EUV radiation. Using a one-dimensional, globally averaged model of the thermosphere and upper mesosphere, *Fuller-Rowell* [1993] indicated that the production of NO is expected to change in response to solar EUV radiation through the solar cycle and over solar rotations. Evidently, it could be possible to improve predictions of the thermosphere's cooling rate as used in the method presented here by incorporating solar EUV indices into the calculation of NO production.

6. Summary and Conclusions

[55] It is often difficult to compare satellite drag-derived atmospheric density measurements taken at different altitudes and orbit locations with each other; comparing the measured densities with the influx of energy from the solar wind is even more challenging. Section 3 of this paper describes a technique by which a proxy temperature correction for the global average thermospheric temperature, ΔT_c, is calculated from density measurements through use of the JB2008 model in a backward manner. These ΔT_c measurements are useful for comparing results from different satellites with each other. It is possible that CHAMP and GRACE data could be used to derive ΔT_c just for the purpose of measuring global temperature and energy changes for event studies; use of the solar wind data and heating models are not required for this measurement.

[56] The W05 empirical model can calculate the total auroral heating in the high-latitude polar caps on the basis of the solar wind and IMF measured upstream of the magnetosphere's bow shock. It has been shown that this heating can be used in a simple differential equation to calculate the resulting changes to T_c in the thermosphere. The numerical coefficients were compared with the total changes in total thermospheric energy content as derived from the J77 model. The results indicate that the energy input into the system, as derived from the W05 model, and with allowances for auroral particle energy, closely matches the thermosphere's change in energy. At levels over 500 GW, the model results are too high and an additional, nonlinear "saturation" correction is required. Additional heating from the small-scale structure in the ionospheric electric field seems to be unnecessary to account for the total energy flow.

[57] The numerical prediction formula includes a time constant for an exponential cooling of the thermosphere. It was found that the cooling is faster (smaller time constant) during and following time periods with extremely high Poynting flux. It is thought that the accelerated cooling is the result of extra NO that is produced as a by-product of both the enhanced auroral particle precipitation and the global heating. The experimental evidence documented by *Barth et al.* [2009], *Barth* [2010], and *Lu et al.* [2010] support this hypothesis.

[58] A very simple model of NO production and decay is included in the numerical difference model. After further analysis, it may be possible to assign actual units to the ΔNO values in the numerical difference equations. Further improvements in the numerical prediction equations may be possible through the inclusion of solar EUV indices in the production of NO.

[59] The calculations described here employ fundamental thermodynamic principles, where the total energy in the thermosphere responds to the total flow of energy into and out from the system. Many physical processes that occur within the system as a whole are not explicitly included in these formulas. On the other hand, there exist several numerical models that are based entirely on physical principles, such as the Coupled Thermosphere Ionosphere Plasmasphere model [*Millward et al.*, 1996].*Doornbos et al.* [2009] compared GRACE and CHAMP measurements with the most recent version of this model that includes electrodynamics (CTIPe), which they consider to be one of the most advanced of the physical models. *Doornbos et al.* [2009, p. 176] had found the following:

> The CTIPe results show an even higher degree of fine detail, compared to the two empirical models, and further approaches the structure seen in the satellite data. A significant difference is in the absolute density values, where CTIPe is of the order 40% higher than either the NRLMSISE-00 or the JB2008 model. There also seems to be a gradient from pole to pole in the CTIPe data that is not apparent in the satellite data and empirical models.

[60] The JB2008 model had the highest correlation with the measurements, and all empirical models performed better than CTIPe [*Doornbos et al.*, 2009]. At this time, physics-based models are not yet able to perform any better than empirical models in tests with actual data.

[61] Comparisons with atmospheric drag measurements on the CHAMP and GRACE satellites show that the temperature calculations from W05 have average errors in the range of 9.7 to 32.8°K (where the total value of T_C is of the order of 1000°K) and correlation coefficients ranging from 0.81 to 0.95. Measurements of the IMF with the ACE satellite are available with a lead time of approximately 1 hour before magnetic field changes impact the Earth's magnetosphere; therefore, it will be possible to predict thermospheric temperature changes in advance through the use of these methods. This could result in improved tracking of satellite debris.

[62] Although the prediction method described here has a high correlation with the orbit averaged thermospheric temperatures, at smaller timescales the satellite measurements show spatial and temporal variations that are more

complex. At auroral latitudes, localized thermospheric density enhancements are seen almost immediately after the onset of increased polar heating. Densities are observed to markedly increase throughout entire orbits with half an hour. Studying this quick spatial and temporal response is a topic for further study.

[63] The ΔT_c temperature correction from the W05 Poynting flux can be used as a direct substitute for the *Dst*-derived correction that is presently used in the JB2008 model; the results shown in Tables 2 and 3 indicate that the accuracy of the JB2008 could be improved through use of this alternative calculation of ΔT_c. Using the W05 model with real-time IMF will also result in predictions that are more timely than those needing to use the *Dst* index. As the future continuity of upstream solar wind and IMF measurements is not guaranteed, the derivation of the corrections from the *Dst* index could be useful as a backup. Efforts are underway to derive a real-time substitute for the traditional method for deriving *Dst* [*Burke et al.*, 2010]. The original JB2008 model had previously been tested through comparisons with drag information from radar and optical tracking of 75 to 80 inactive "calibration satellites" [*Bowman et al.*, 2008a]. A future step, beyond the scope of this paper, should include similar tests where the Poynting flux calculations of the ΔT_c correction are used in JB2008 model comparisons with satellites other than CHAMP and GRACE.

[64] **Acknowledgments.** This work is funded by the NASA Living With a Star Program through grant NNX09AJ58G to Virginia Polytechnic Institute and State University.

[65] Robert Lysak thanks the reviewers for their assistance in evaluating this paper.

References

Anderson, B. J., J. B. Gary, T. A. Potemra, R. A. Frahm, J. R. Sharber, and J. D. Winningham (1998), UARS observations of Birkeland currents and Joule heating rates from the November 4, 1993, storm, *J. Geophys. Res.*, *103*(A11), 26,323–26,335, doi:10.1029/98JA01236.

Bailey, S. M., C. A. Barth, and S. C. Solomon (2002), A model of nitric oxide in the lower thermosphere, *J. Geophys. Res.*, *107*(A8), 1205, doi:10.1029/2001JA000258.

Barth, C. A. (2010), Joule heating and nitric oxide in the thermosphere, 2, *J. Geophys. Res.*, *115*, A10305, doi:10.1029/2010JA015565.

Barth, C. A., W. K. Tobiska, D. E. Siskind, and D. D. Cleary (1988), Solar-terrestrial coupling: Low-latitude thermospheric nitric oxide, *Geophys. Res. Lett.*, *15*, 92–94, doi:10.1029/GL015i001p00092.

Barth, C. A., K. D. Mankoff, S. M. Bailey, and S. C. Solomon (2003), Global observations of nitric oxide in the thermosphere, *J. Geophys. Res.*, *108*(A1), 1027, doi:10.1029/2002JA009458.

Barth, C. A., G. Lu, and R. G. Roble (2009), Joule heating and nitric oxide in the thermosphere, *J. Geophys. Res.*, *114*, A05301, doi:10.1029/2008JA013765.

Bowman, B. R., W. K. Tobiska, and F. A. Marcos (2006), A new empirical thermospheric density model JB2006 using new solar indices, *Paper 2006-6166*, Am. Inst. of Aeronaut. and Astronaut., New York.

Bowman, B. R., W. K. Tobiska, F. A. Marcos, C. Y. Huang, C. S. Lin, and W. J. Burke (2008a), A new empirical thermospheric density model JB2008 using new solar and geomagnetic indices, *Paper 2008-6438*, Am. Inst. of Aeronaut. and Astronaut., New York.

Bowman, B. R., W. K. Tobiska, F. A. Marcos, and C. Valladares (2008b), The JB2006 empirical thermospheric density model, *J. Atmos. Sol. Terr. Phys.*, *70*, 774–793.

Bruinsma, S., D. Tamagnan, and R. Biancale (2004), Atmospheric densities derived from CHAMP/STAR accelerometer observations, *Planet. Space Sci.*, *52*, 297–312.

Bruinsma, S., J. M. Forbes, R. S. Nerem, and X. Zhang (2006), Thermosphere density response to the 20–21 November 2003 solar and geomagnetic storm from CHAMP and GRACE accelerometer data, *J. Geophys. Res.*, *111*, A06303, doi:10.1029/2005JA011284.

Burke, W. J. (2007), Penetration electric fields: A Volland-Stern approach, *J. Atmos. Sol. Terr. Phys.*, *69*, 1114–1126.

Burke, W. J. (2008), Stormtime energy budgets of the global thermosphere, in *Mid-Latitude Ionospheric Dynamics and Disturbances*, *Geophys. Monogr. Ser.*, vol. 181, edited by P. M. Kintner et al., pp. 235–246, AGU, Washington, D. C.

Burke, W. J., C. Y. Huang, F. A. Marcos, and J. O. Wise (2007), Interplanetary control of thermospheric densities during large magnetic storms, *J. Atmos. Sol. Terr. Phys.*, *69*, 279–287, doi:10.1016/j.jastp.2006.05.027.

Burke, W. J., C. S. Lin, M. P. Hagan, C. Y. Huang, D. R. Weimer, J. O. Wise, L. C. Gentile, and F. A. Marcos (2009), Stormtime global thermosphere: A driven-dissipative thermodynamic system, *J. Geophys. Res.*, *114*, A06306, doi:10.1029/2008JA013848.

Burke, W. J., G. R. Wilson, C. S. Lin, F. J. Rich, J. O. Wise, and M. P. Hagan (2010), Estimating Dst indices and exospheric temperatures from equatorial magnetic fields measured by DMSP satellites, *J. Geophys. Res.*, doi:10.1029/2010JA015310, in press.

Casali, S. J., and W. N. Barker (2002), Dynamic calibration atmosphere (DCA) for the high accuracy satellite drag model (HASDM), *Paper 2002-4888*, Am. Inst. of Aeronaut. and Astronaut., New York.

Chun, F. K., D. J. Knipp, M. G. McHarg, G. Lu, B. A. Emery, S. Vennerstrom, and O. A. Troshichev (1999), Polar cap index as a proxy for hemispheric Joule heating, *Geophys. Res. Lett.*, *26*(8), 1101–1104, doi:10.1029/1999GL900196.

Chun, F. K., D. J. Knipp, M. G. McHarg, J. R. Lacey, G. Lu, and B. A. Emery (2002), Joule heating patterns as a function of polar cap index, *J. Geophys. Res.*, *107*(A7), 1119, doi:10.1029/2001JA000246.

Codrescu, M. V., T. J. Fuller-Rowell, and J. C. Foster (1995), On the importance of E-field variability for Joule heating in the high-latitude thermosphere, *Geophys. Res. Lett.*, *22*, 2393–2396, doi:10.1029/95GL01909.

Cosgrove, R. B., G. Lu, H. Bahcivan, T. Matsuo, C. J. Heinselman, and M. A. McCready (2009), Comparison of AMIE-modeled and Sondrestrom-measured Joule heating: A study in model resolution and electric field–conductivity correlation, *J. Geophys. Res.*, *114*, A04316, doi:10.1029/2008JA013508.

Crowley, G., D. J. Knipp, K. A. Drake, J. Lei, E. Sutton, and H. Lühr (2010), Thermospheric density enhancements in the dayside cusp region during strong by conditions, *Geophys. Res. Lett.*, *37*, L07110, doi:10.1029/2009GL042143.

Deng, Y., A. Maute, A. D. Richmond, and R. G. Roble (2008), Analysis of thermospheric response to magnetospheric inputs, *J. Geophys. Res.*, *113*, A04301, doi:10.1029/2007JA012840.

Doornbos, E., M. Frster, B. Fritsche, T. van Helleputte, J. van den IJssel, G. Koppenwallner, H. Luhr, D. Rees, and P. Visser (2009), Air density models derived from multi-satellite drag observations, *Tech. Rep.*, Delft Inst. of Earth Obs. and Space Syst., Eur. Space Agency, Delft, Netherlands.

Duff, J. W., H. Dothe, and R. D. Sharma (2003), On the rate coefficient of the $N(2D)+O_2 \rightarrow NO+O$ reaction in the terrestrial thermosphere, *Geophys. Res. Lett.*, *30*(5), 1259, doi:10.1029/2002GL016720.

Emery, B. A., C. Lathuillere, P. G. Richards, R. G. Roble, M. J. Buonsanto, D. J. Knipp, P. Wilkinson, D. P. Sipler, and R. Niciejewski (1999), Time dependent thermospheric neutral response to the 2–11 November 1993 storm period, *J. Atmos. Sol. Terr. Phys.*, *61*, 329–350.

Fairfield, D. H. (1971), Average and unusual locations of the Earth's magnetopause and bow shock, *J. Geophys. Res.*, *76*(28), 6700–6716, doi:10.1029/JA076i028p06700.

Fuller-Rowell, T. (1993), Modeling the solar cycle change in nitric oxide in the thermosphere and upper mesosphere, *J. Geophys. Res.*, *98*(A2), 1559–1570, doi:10.1029/92JA02201.

Gopalswamy, N., L. Barbieri, E. W. Cliver, G. Lu, S. P. Plunkett, and R. M. Skoug (2005), Introduction to violent Sun-Earth connection events of October–November 2003, *J. Geophys. Res.*, *110*, A09S00, doi:10.1029/2005JA011268.

Haines, G. V. (1985), Spherical cap harmonic analysis, *J. Geophys. Res.*, *90*(B3), 2583–2591, doi:10.1029/JB090iB03p02583.

Hill, T. W., A. Dessler, and R. A. Wolf (1976), Mercury and Mars: The role of ionospheric conductivity in the acceleration of magnetospheric particles, *Geophys. Res. Lett.*, *3*, 429–432, doi:10.1029/GL003i008p00429.

Jacchia, L. G. (1970), New static models of the thermosphere and exosphere with empirical temperature profiles, *Tech. Rep. Spec. Rep. 313*, Smithsonian Astrophys. Obs., Cambridge, Mass.

Jacchia, L. G. (1977), Thermospheric temperature density and composition: A new model, *Tech. Rep. Spec. Rep. 375*, Smithsonian Astrophys. Obs., Cambridge, Mass.

Johnson, E. S., and R. A. Heelis (2005), Characteristics of ion velocity structure at high latitudes during steady southward IMF conditions, *J. Geophys. Res.*, *110*, A12301, doi:10.1029/2005JA011130.

Knipp, D. J., W. K. Tobiska, and B. A. Emery (2004), Direct and indirect thermospheric heating sources for solar cycles 21–23, *Sol. Phys.*, *224*, 495–505.

Lu, G., A. D. Richmond, B. A. Emery, and R. G. Roble (1995), Magnetosphere-ionosphere-thermosphere coupling: Effect of neutral wind on energy transfer and field-aligned current, *J. Geophys. Res.*, *100*(A10), 19,643–19,659, doi:10.1029/95JA00766.

Lu, G., et al. (1998), Global energy deposition during the January 1997 magnetic cloud event, *J. Geophys. Res.*, *103*(A6), 11,685–11,694, doi:10.1029/98JA00897.

Lu, G., M. G. Mlynczak, L. A. Hunt, T. N. Woods, and R. G. Roble (2010), On the relationship of Joule heating and nitric oxide radiative cooling in the thermosphere, *J. Geophys. Res.*, *115*, A05306, doi:10.1029/2009JA014662.

Marsh, D. R., S. C. Solomon, and A. E. Reynolds (2004), Empirical model of nitric oxide in the lower thermosphere, *J. Geophys. Res.*, *109*, A07301, doi:10.1029/2003JA010199.

Matsuo, T., and A. D. Richmond (2008), Effects of high-latitude ionospheric electric field variability on global thermospheric Joule heating and mechanical energy transfer rate, *J. Geophys. Res.*, *113*, A07309, doi:10.1029/2007JA012993.

Matsuo, T., A. D. Richmond, and K. Hensel (2003), High-latitude ionospheric electric field variability and electric potential derived from DE-2 plasma drift measurements: Dependence on IMF and dipole tilt, *J. Geophys. Res.*, *108*(A1), 1005, doi:10.1029/2002JA009429.

McComas, D. J., S. J. Bame, P. Barber, W. C. Feldman, J. L. Phillips, and P. Riley (1998), Solar wind electron, proton, and alpha monitor (SWEPAM) on the Advanced Composition Explorer, *Space Sci. Rev.*, *86*, 563–612.

McHarg, M., F. Chun, D. Knipp, G. Lu, B. Emery, and A. Ridley (2005), High-latitude Joule heating response to IMF inputs, *J. Geophys. Res.*, *110*, A08309, doi:10.1029/2004JA010949.

Millward, G. H., H. Rishbeth, T. Fuller-Rowell, A. Aylward, S. Quegan, and R. Moffett (1996), Ionospheric F_2 layer seasonal and semiannual variations, *J. Geophys. Res.*, *101*(A3), 5149–5156, doi:10.1029/95JA03343.

Mlynczak, M. G., et al. (2005), Energy transport in the thermosphere during the solar storms of April 2002, *J. Geophys. Res.*, *110*, A12S25, doi:10.1029/2005JA011141.

Press, W. H., B. P. Flannery, S. A. Teukolsky, and W. T. Vetterling (1986), Numerical Recipes: The Art of Scientific Computing, Cambridge Univ. Press, New York.

Richmond, A. D. (1992), Assimilative mapping of ionospheric electrodynamics, *Adv. Space Res.*, *6*, 59–68.

Richmond, A. D., et al. (1990), Global measures of ionospheric electrodynamic activity inferred from combined incoherent scatter radar and ground magnetometer observations, *J. Geophys. Res.*, *95*(A2), 1061–1071, doi:10.1029/JA095iA02p01061.

Sætre, C., C. A. Barth, J. Stadsnes, N. Østgaard, S. M. Bailey, D. N. Baker, G. A. Germany, and J. W. Gjerloev (2007), Thermospheric nitric oxide at higher latitudes: Model calculations with auroral energy input, *J. Geophys. Res.*, *112*, A08306, doi:10.1029/2006JA012203.

Schlegel, K., H. Lühr, J.-P. St.-Maurice, G. Crowley, and C. Hackert (2005), Thermospheric density structures over the polar regions observed with CHAMP, *Ann. Geophys.*, *23*, 1659–1672.

Sharma, R. D., H. Dothe, F. von Esse, V. A. Kharchenko, Y. Sun, and A. Dalgarno (1996), Production of vibrationally and rotationally excited NO in the night time terrestrial thermosphere, *J. Geophys. Res.*, *101*(A9), 19,707–19,713, doi:10.1029/96JA01004.

Shepherd, S. G. (2007), Polar cap potential saturation: Observations, theory, and modeling, *J. Atmos. Sol. Terr. Phys.*, *69*, 234–248.

Siscoe, G. L., G. M. Erickson, B. U. O. Sonnerup, N. C. Maynard, J. A. Schoendorf, K. D. Siebert, D. R. Weimer, W. W. White, and G. R. Wilson (2002), Hill model of transpolar potential saturation: Comparisons with MHD simulations, *J. Geophys. Res.*, *107*(A6), 1075, doi:10.1029/2001JA000109.

Siskind, D., C. Barth, D. Evans, and R. Roble (1989), The response of thermospheric nitric oxide to an auroral storm: 2. Auroral latitudes, *J. Geophys. Res.*, *94*(A12), 16,899–16,911, doi:10.1029/JA094iA12p16899.

Skoug, R. M., J. T. Gosling, J. T. Steinberg, D. J. McComas, C. W. Smith, N. F. Ness, Q. Hu, and L. F. Burlaga (2004), Extremely high speed solar wind: 29–30 October 2003, *J. Geophys. Res.*, *109*, A09102, doi:10.1029/2004JA010494.

Smith, C. W., M. H. Acuna, L. F. Burlaga, J. L. N. F. Ness, and J. Scheifele (1998), The ACE magnetic field experiment, *Space Sci. Rev.*, *86*, 613–632.

Solomon, S. C., T. N. Woods, L. V. Didkovsky, J. T. Emmert, and L. Qian (2010), Anomalously low solar extreme-ultraviolet irradiance and thermospheric density during solar minimum, *Geophys. Res. Lett.*, *37*, L16103, doi:10.1029/2010GL044468.

Song, P., V. M. Vasyliunas, and L. Ma (2005), Solar wind-magnetosphere-ionosphere coupling: Neutral atmosphere effects on signal propagation, *J. Geophys. Res.*, *110*, A09309, doi:10.1029/2005JA011139.

Storz, M. F., B. R. Bowman, and M. J. I. Branson (2002), High accuracy satellite drag model (HASDM), *Paper 2002-4888*, Am. Inst. of Aeronaut. and Astronaut., New York.

Sutton, E. K., J. M. Forbes, and R. S. Nerem (2005), Global thermospheric neutral density and wind response to the severe 2003 geomagnetic storms from CHAMP accelerometer data, *J. Geophys. Res.*, *110*, A09S40, doi:10.1029/2004JA010985.

Sutton, E. K., R. S. Nerem, and J. M. Forbes (2007), Density and winds in the thermosphere deduced from accelerometer data, *J. Spacecr. Rockets*, *44*(6), 1210–1219, doi:10.2514/1.28641.

Sutton, E. K., J. M. Forbes, and D. J. Knipp (2009), Rapid response of the thermosphere to variations in Joule heating, *J. Geophys. Res.*, *114*, A04319, doi:10.1029/2008JA013667.

Tapley, B. D., S. B. M. Watkins, and C. Reigber (2004), The gravity recovery and climate experiment: Mission overview and early results, *Geophys. Res. Lett.*, *31*, L17S05, doi:10.1029/2004GL019929.

Tobiska, W. K., S. D. Bouwer, and B. R. Bowman (2008), The development of new solar indices for use in thermospheric density modeling, *J. Atmos. Sol. Terr. Phys.*, *70*, 803–819.

Vasyliunas, V. M., and P. Song (2005), Meaning of ionospheric Joule heating, *J. Geophys. Res.*, *110*, A02301, doi:10.1029/2004JA010615.

Weimer, D. R. (2005a), Predicting surface geomagnetic variations using ionospheric electrodynamic models, *J. Geophys. Res.*, *110*, A12307, doi:10.1029/2005JA011270.

Weimer, D. R. (2005b), Improved ionospheric electrodynamic models and application to calculating Joule heating rates, *J. Geophys. Res.*, *110*, A05306, doi:10.1029/2004JA010884.

Weimer, D. R., and J. H. King (2008), Improved calculations of interplanetary magnetic field phase front angles and propagation time delays, *J. Geophys. Res.*, *113*, A01105, doi:10.1029/2007JA012452.

Weimer, D. R., C. R. Clauer, M. J. Engebretson, T. L. Hansen, H. Gleisner, I. Mann, and K. Yumoto (2010), Statistical maps of geomagnetic variations as a function of the interplanetary magnetic field, *J. Geophys. Res.*, *115*, A10320, doi:10.1029/2010JA015540.

Wilson, G. R., D. R. Weimer, J. O. Wise, and F. A. Marcos (2006), Response of the thermosphere to Joule heating and particle precipitation, *J. Geophys. Res.*, *111*, A10314, doi:10.1029/2005JA011274.

Wright, D. (2007), Space debris, *Phys. Today*, *60*(10), 35–40.

B. R. Bowman, Air Force Space Command, Peterson AFB, 250 S. Peterson Blvd., Ste. 116, Colorado Springs, CO 80925, USA. (bruce.bowman@peterson.af.mil)

E. K. Sutton, Air Force Research Laboratory, Hanscom AFB, Bedford, MA 01730, USA. (eric.sutton@hanscom.af.mil)

W. K. Tobiska, Space Environment Technologies, 1676 Palisades Dr., Pacific Palisades, CA 90272, USA. (ktobiska@spacenvironment.net)

D. R. Weimer, National Institute of Aerospace, Virginia Polytechnic Institute and State University, 100 Exploration Way, Hampton, VA 23666, USA. (dweimer@vt.edu)